Structural and electrical properties of *c*-axis epitaxial homologous $Sr_{m-3}Bi_4Ti_mO_{3m+3}$ ($m=3$, 4, 5, and 6) thin films

S. T. Zhang and Y. F. Chen[a)]
National Laboratory of Solid State Microstructures and Department of Materials Science and Engineering, Nanjing University, Nanjing 210093, People's Republic of China

H. P. Sun and X. Q. Pan
Department of Materials Science and Engineering, University of Michigan, Ann Arbor, Michigan 48109

W. S. Tan
National Laboratory of Solid State Microstructures and Department of Physics, Nanjing University, Nanjing 210093, People's Republic of China

Z. G. Liu and N. B. Ming
National Laboratory of Solid State Microstructures and Department of Materials Science and Engineering, Nanjing University, Nanjing 210093, People's Republic of China

(Received 3 February 2003; accepted 15 April 2003)

c-axis epitaxial thin films of Bi-layered homologous $Sr_{m-3}Bi_4Ti_mO_{3m+3}$ ($m=3$, 4, 5, and 6) were fabricated on (001) $SrTiO_3$ single crystal substrates by pulsed laser deposition, respectively. Microstructures of the films were systematically characterized by x-ray diffraction (including θ–2θ scans, rocking curve scans and ϕ scans), atomic force microscopy, and transmission electron microscope. Epitaxial relations were established to be $(001)Sr_{m-3}Bi_4Ti_mO_{3m+3}\|(001)SrTiO_3$ and $[1\bar{1}0]Sr_{m-3}Bi_4Ti_mO_{3m+3}\|[010]SrTiO_3$ by ϕ scans and selected area diffraction. A special kind of atomic shift along the [001] direction and a slight atomic vibration of TiO_6 octahedra were revealed and discussed. The room-temperature dielectric constants of these epitaxial films measured by using an evanescent microwave probe were 245 ± 23, 237 ± 13, 272 ± 19, and 221 ± 20 for films with $m=3$, 4, 5, and 6 respectively. © *2003 American Institute of Physics.* [DOI: 10.1063/1.1579864]

I. INTRODUCTION

There has been much interest in ferroelectric thin films since their unique dielectric, piezoelectric, pyroelectric, and ferroelectric properties can be utilized for memory devices, ultrasonic sensors, and infrared detectors.[1–3] In recent years, electrical properties of Bi-layered oxides (Aurivillius phases) such as $SrBi_2Ta_2O_9$ (SBT) and $Bi_{4-x}La_xTi_3O_{12}$ thin films have been widely studied for their applications in nonvolatile ferroelectric random access memory (NVFRAM).[4–6] The Bi-layered oxide family can be described as $(Bi_2O_2)^{2+}(A_{m-1}B_mO_{3m+1})^{-2}$, where A represents Bi, Ba, Pb, Sr, Ca, K, Na, and rare earth elements, B represents Ti, Ta, Nb, W, Mo, Fe, etc., and *m* represents the number of BO_6 octahedra between two neighboring Bi_2O_2 layers. For example, SBT ($m=2$), $Bi_4Ti_3O_{12}$ (BTO, $m=3$), $SrBi_4Ti_4O_{15}$ ($SBTi_4$, $m=4$) and $Sr_2Bi_4Ti_5O_{18}$ ($SBTi_5$, $m=5$) have 2, 3, 4, and 5 octahedra, respectively. Electrical properties of polycrystalline thin films of these materials in capacitor structures with simple metal electrodes have been well studied.[4,7] However, reports on microstructure and electrical properties of *a*-, *b*-, and *c*-axis epitaxial thin films of these oxides are rare in literature though such epitaxial-thin-film/substrate systems are important in the development of device applications, as well as in fundamental issues such as in interface physics and growth mechanisms of artificial structures. This is because for these highly anisotropic oxides, the *a*- and *b*-axis epitaxial films are very difficult to fabricate, and although the *c*-axis epitaxial films are easy to fabricate, in view of NVFRAM application, the *c*-axis epitaxial films are of little significance since the vector of the spontaneous polarization is perpendicular to the *c* axis, specifically along the *a* axis.[8–10] However, in view of academic point, many important physical, chemical, and structural properties of these Bi-layered oxides remain to be further investigated. Probing *c*-axis epitaxial films of these rather unconventional materials can reveal the fundamental structural properties since such studies are important for understanding the basic structure and intrinsic properties.[11] It should be noted that, very recently, Chon *et al.* reported that by suitably substituting trivalent ions, the Ti-based Bi-layered oxides show giant spontaneous polarization along *c*-axis direction.[12] Therefore, growing and probing the *c*-axis epitaxial films of the Bi-layered oxides are still of great importance.

On the other hand, it was suggested that Bi-layered oxides with $m>5$ could not occur naturally and some attempts to fabricate such an oxide ended in a mixture of the phase $SBTi_5$ and $SrTiO_3$.[13] However, there is no direct reason to prohibit their occurrence, especially in the form of thin films. In the case of $Sr_3Bi_4Ti_6O_{21}$ ($SBTi_6$) which should have six octahedra blocks between two neighboring $(Bi_2O_2)^{2+}$ layers, although its optical properties have been reported,[14] there is, as far as we know, no careful structural characterization [i.e., high-resolution transmission electron micro-

a)Electronic mail: yfchen@nju.edu.cn

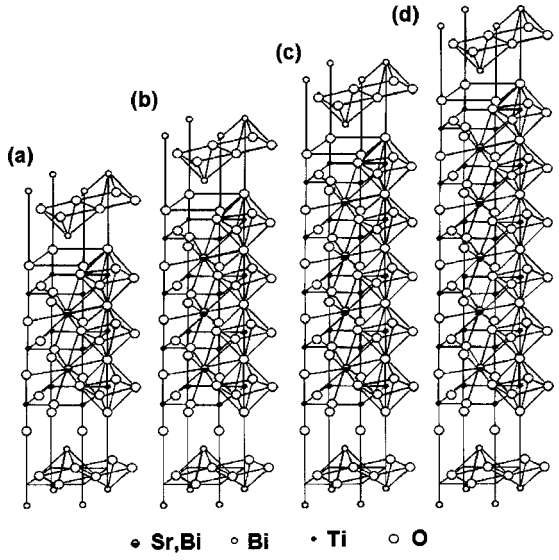

FIG. 1. Schematic of the crystal structure of (a) BTO, (b) $SBTi_4$, (c) $SBTi_5$, and (d) $SBTi_6$.

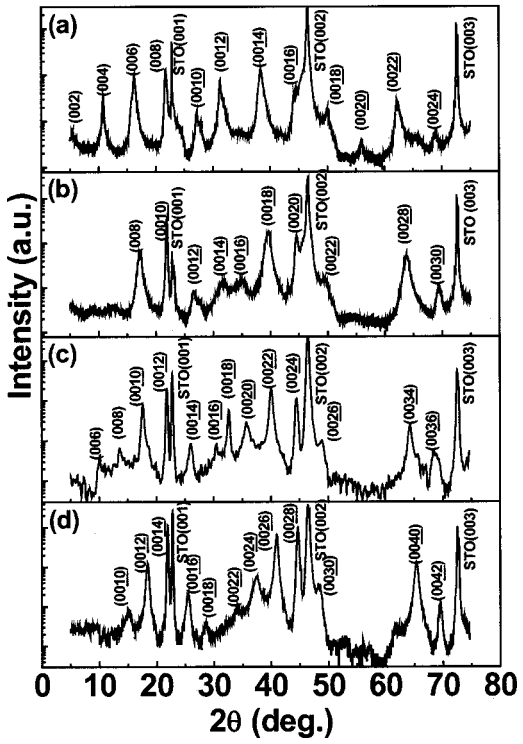

FIG. 2. XRD θ–2θ scans patterns of the films deposited on (001) STO single-crystal substrates: (a) $m=3$, (b) $m=4$, (c) $m=5$, and (d) $m=6$.

scope (HRTEM)] of it have been carried out to ensure a single phase material. To meet this goal, HRTEM studies of *c*-axis epitaxial $SBTi_6$ thin films are necessary.

The synthesis of homologous oxide thin films system can offer tremendous potential for tailoring the ferroelectric and dielectric properties of materials. For example, by preparing the first five members of the $Sr_{n+1}Ti_nO_{3n+1}$ ruddlesden–popper homologous series by molecular beam epitaxy (MBE), Haeni *et al.* reveal that the first member of this series, Sr_2TiO_4, has several potential advantages over the $n=\infty$ member, $SrTiO_3$, in the applications of metal-oxide-semiconductor field effect transistors (MOSFETs).[15]

Motivated by the works described above, we prepared *c*-axis epitaxial homologous BTO, $SBTi_4$, $SBTi_5$, and $SBTi_6$ thin films on (001)$SrTiO_3$ (STO) single crystal substrates by pulsed laser deposition (PLD) and studied their microstructures and electrical properties. BTO $SBTi_4$, $SBTi_5$, and $SBTi_6$ are four members of the Bi-layered oxide family with 3, 4, 5, and 6 TiO_6 octahedra between two neighboring Bi_2O_2 layers, respectively. The schematic of the crystal structure of these Bi-layered materials are shown in Figs. 1(a)–1(d).

According to Hesse *et al.*,[16] for Bi-layered oxides, the pseudotetragonal or the orthorhombic structure can be used. In the case of pseudotetragonal structure, the *a*- and *b*- lattice constants of these materials are about 3.84–3.86 Å, which show little variation with respect to *m* value and are very similar with the lattice constant of cubic STO ($a=3.90$ Å) and that of pseudocubic $LaAlO_3$ (LAO, $a=3.79$ Å). The lattice mismatches of these materials between STO are less than 1.54% and between LAO are less than 1.32%, therefore, STO and LAO are promising substrates for the *c*-axis epitaxial growth of $Sr_{m-3}Bi_4Ti_mO_{3m+3}$ ($m=3$, 4, 5, and 6) thin films. In this article, however, orthorhombic structure indexing will be used.

II. EXPERIMENTAL DETAILS

Ceramic pellet of BTO used as the PLD target was prepared by a citrate complex method and that of $SBTi_m$ ($m=4$, 5, and 6) was prepared by solid-state reaction, respectively. The preparation details were discussed elsewhere.[7] The PLD processes were performed using a KrF excimer laser of wavelength of 248 nm, pulsewidth of 30 ns. The BTO and $SBTi_m$ ($m=4$, 5, and 6) thin films were fabricated at 750 °C on (001) STO single crystal substrates for 20 min, respectively. During each fabrication, the flowing oxygen pressure was 30 Pa and deposition frequency was 5 Hz. After each fabrication, film was *in situ* annealed at 750 °C with 0.5 atmosphere oxygen pressure for 10 min.

The crystal structures and epitaxial arrangements of the films were studied by x-ray diffraction (XRD) using a Rigaku-D/Max-rA diffractometer and a SIEMENS D5000 diffractometer. Surface morphologies and cross-sectional microstructures were examined by a Nanoscope IIIa atomic force microscopy (AFM) and a JEOL 4000EX transmission electron microscope, respectively. Room temperature dielectric constants were measured by using an evanescent microwave probe (EMP).[17,18]

III. STRUCTURE CHARACTERIZATION

A. XRD study

Figures 2(a)–2(d) show the XRD patterns of BTO and $SBTi_m$ ($m=4$, 5, and 6) films deposited on (001) STO single crystal substrates, respectively. The peaks of BTO, $SBTi_4$, and $SBTi_5$ were indexed according to the standard powder diffraction data while the peaks of $SBTi_6$ are indexed by

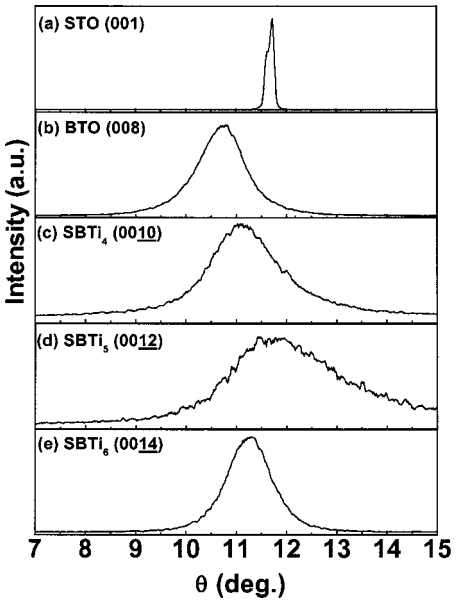

FIG. 3. XRD rocking curves of the (a) STO substrate and (b) BTO, (c) $SBTi_4$, (d) $SBTi_5$, and (e) $SBTi_6$.

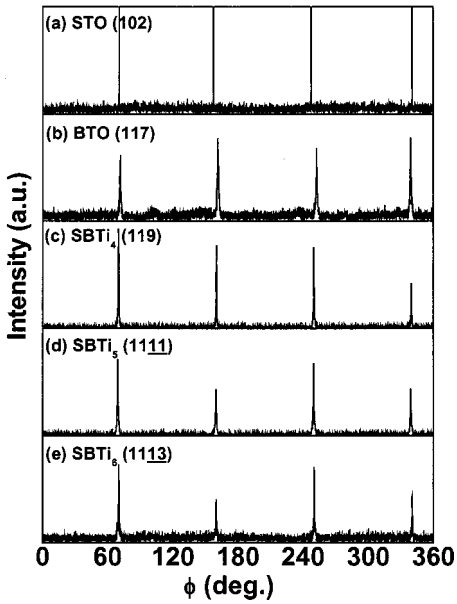

FIG. 4. XRD ϕ scans patterns of the (a) STO substrate and (b) BTO, (c) $SBTi_4$, (d) $SBTi_5$, and (e) $SBTi_6$.

assuming $c=5.700$ nm.[14] Obviously, only $(00l)$ peaks of these materials and $(00l)$ peaks of STO substrates can be detected, indicating the highly *c*-axis oriented growth of these films.

To detect if there is a tilt of *c*-axis orientation away from the surface normal, rocking curve measurements of STO (001) reflection and BTO (008), $SBTi_4$ $(00\underline{1}0)$, $SBTi_5$ $(00\underline{1}2)$, and $SBTi_6$ $(00\underline{1}4)$ reflections were carried out. The results are shown in Figs. 3(a)–3(e). The full width at half maximum (FWHM) of (001) reflection of STO substrate and (008), $(00\underline{1}0)$, $(00\underline{1}2)$, and $(00\underline{1}4)$ reflections of BTO, $SBTi_4$, $SBTi_5$, $SBTi_6$ films were 0.17°, 0.95°, 1.41°, 2.34°, and 1.01°, respectively, implying that high quality *c*-axis textured films have been prepared.

X-ray ϕ scans were employed to investigate the epitaxial qualities and epitaxial behaviors of these films. In the ϕ scan measurements, STO (102), BTO (117), $SBTi_4$ (119), $SBTi_5$ $(11\underline{1}1)$, and $SBTi_6$ $(11\underline{1}3)$ reflections were selected. For each measurement, the 2θ and ψ, the tilt angle off the surface normal, were fixed at defined values, as shown in Table I. Then the corresponding ϕ scan result was obtained by rotating the sample 0°–360°. The results were plotted in Figs. 4(a)–4(e). The measured FWHM of STO (102), BTO (117), $SBTi_4$ (119), $SBTi_5$ $(11\underline{1}1)$, and $SBTi_6$ $(11\underline{1}3)$ reflections are 0.12°, 1.12°, 0.53°, 0.85°, and 0.41°, respectively. In Fig. 4(a), four equally spaced peaks separated by 90° could be observed, as was expected for cubic STO. In each case of Figs. 4(b)–4(e), four peaks separated by about 90° indicating that the *c* axis is the fourfold symmetric axis of these materials. The in-plane lattice of BTO, $SBTi_4$, $SBTi_5$, and $SBTi_6$ are believed to be restricted by the substrate lattice, to form a pseudomorphic tetragonal structure without orthogonal distortion.[19] The angles between STO (102) and BTO (117), $SBTi_4$ (119), $SBTi_5$ $(11\underline{1}1)$, and $SBTi_6$ $(11\underline{1}3)$ reflections are all about 0°, which is almost equal to the calculated values. From these results, the alignment of the in-plane lattice vectors can be concluded. Therefore, the epitaxial relation is established to be

$$(001)\mathrm{Sr}_{m-3}\mathrm{Bi}_4\mathrm{Ti}_m\mathrm{O}_{3m+3}\|(001)\mathrm{STO},$$
$$[110]\mathrm{Sr}_{m-3}\mathrm{Bi}_4\mathrm{Ti}_m\mathrm{O}_{3m+3}\|[100]\mathrm{STO},$$

and

$$[1\bar{1}0]\mathrm{Sr}_{m-3}\mathrm{Bi}_4\mathrm{Ti}_m\mathrm{O}_{3m+3}\|[010]\mathrm{STO}.$$

TABLE I. Parameters used for x-ray ϕ scans measurements.

	2θ	ψ
STO (102)	52.34°	26.57°
BTO (117)	30.03°	50.62°
$SBTi_4$ (119)	30.10°	49.77°
$SBTi_5$ $(11\underline{1}1)$	30.71°	48.97°
$SBTi_6$ $(11\underline{1}3)$	31.04°	48.44°

B. AFM surface morphologies

AFM surface morphology can provide sufficient information about the growth mode of thin film.[20–23] The surface morphologies of these epitaxial films were recorded by AFM over an area of $3\ \mu\mathrm{m}\times 3\ \mu\mathrm{m}$, as shown in Figs. 5(a)–5(d). Generally, the extremely smooth, dense, and uniform surface without any cracks or voids of BTO film and the relatively rough surface morphologies of $SBTi_4$, $SBTi_5$, and $SBTi_6$ films with some irrational islands were shown. The AFM surface morphologies indicate that the growth mechanism of BTO is different from that of $SBTi_4$, $SBTi_5$, and $SBTi_6$: the BTO film is grown via a two-dimensional (2D) layer-by-layer growth mode[23,24] while the $SBTi_4$, $SBTi_5$, and $SBTi_6$ films have undergone a three-dimensional (3D) island-like growth mode.[22] The different growth mode of BTO, $SBTi_4$, $SBTi_5$, and $SBTi_6$ is also revealed by cross-sectional TEM images, as will be shown in the following. It should be noted

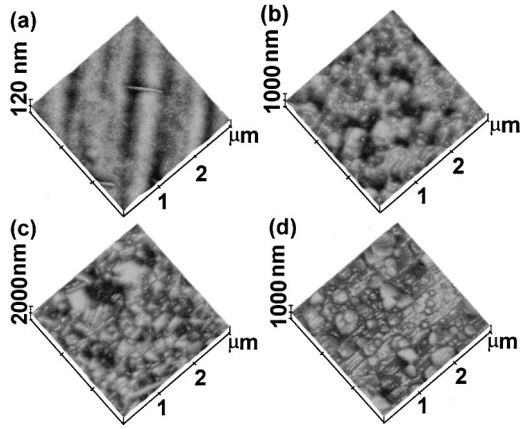

FIG. 5. AFM surface morphologies of (a) BTO, (b) $SBTi_4$, (c) $SBTi_5$, and (d) $SBTi_6$ epitaxial films on STO substrates, respectively.

that in Fig. 5(a), the stripes of the BTO films can be seen, which indicate that the surface of STO substrate can be considered to consist of steps, terraces, and kinks.[25]

C. Cross-sectional TEM studies

Figures 6(a)–6(d) are the low magnification cross-sectional TEM overview micrographs of the BTO/STO, $SBTi_4$/STO, $SBTi_5$/STO, and $SBTi_6$/STO heterostructures, respectively. The BTO film is homologous with no detectable grain boundaries and the interface and surface are sharp enough. This result confirms again that the BTO film is grown via a 2D layer-by-layer growth mode. In the case of SBTi film, the irrational grain boundaries perpendicular to the film normal are presented, which are the typical clues of 3D island growth mode. One of the factors that might be responsible for the different growth mode of BTO and $SBTi_m$ ($m=4$, 5, and 6) is that BTO has only Bi–Ti–O perovskite unit while $SBTi_m$ ($m=4$, 5, and 6) have different Bi–Ti–O and Sr–Ti–O perovskite units. Note that in a Bi-layered material with different perovskite units, the atomic displacement, thus the strain, along *a* or *b* axis is larger than that in such a material with only one kind of perovskite unit.[26]

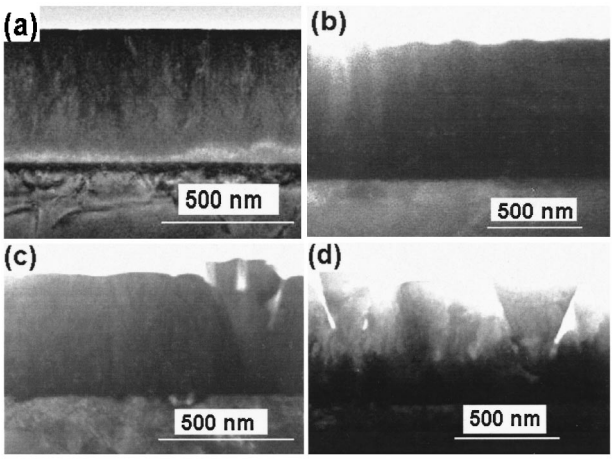

FIG. 6. SEAD patterns of the (a) STO substrate and (b) BTO, (c) $SBTi_4$, (d) $SBTi_5$, and (e) $SBTi_6$.

Therefore, at the early stage of film growth, large strain of $SBTi_m$ ($m=4$, 5, and 6) along the *a* or *b* axis will force the adatoms to form separated *c*-axis epitaxial island, which is 3D island growth mode. In the case of BTO, relatively small strain along the *a* or *b* axis may not be sufficient to force the adatoms to form separated *c*-axis epitaxial island, therefore, BTO film is grown via a 2D layer-by-layer growth mode. These results are consistent with the AFM surface morphology measurements. The average thickness of BTO, $SBTi_4$, $SBTi_5$, and $SBTi_6$ films are 452, 735, 432, and 500 nm, respectively.

The selected area electron diffractions (SAED) of BTO/STO heterostructure are shown in Figs. 7(a)–7(c). Figure 7(a) is a SAED pattern taken from the STO single crystal substrate area along the [010] direction, Fig. 7(b) is a SAED pattern taken in the area of the BTO films, which is identified to be the $[1\bar{1}0]$ zone electron diffraction pattern, and Fig. 7(c) is a SAED pattern taken in the area covering both the film and substrate, which is a simple superposition diffraction pattern of BTO film and STO substrate because typically (001) diffraction spot of STO can also be identified in this figure, as indicated by an arrow. The sharp electron diffraction spots with no broadening again indicate that the film have good single crystallinity. Similar results of $SBTi_4$/STO, $SBTi_5$/STO, and $SBTi_6$/STO heterostructures were also obtained, as shown in Figs. 7(d)–7(f), Figs. 7(h)–7(i), and Figs. 7(j)–7(l), respectively. From these SEAD results, the interface relationship has been found to be

$$(001)\mathrm{Sr}_{m-3}\mathrm{Bi}_4\mathrm{Ti}_m\mathrm{O}_{3m+3}\|(001)\mathrm{STO}$$

and

$$[1\bar{1}0]\mathrm{Sr}_{m-3}\mathrm{Bi}_4\mathrm{Ti}_m\mathrm{O}_{3m+3}\|[010]\mathrm{STO}$$

($m=3$, 4, 5, and 6), which is consistent with the x-ray ϕ scan results.

Figures 8(a)–8(d) show the cross-sectional HRTEM images of the BTO, $SBTi_4$, $SBTi_5$, and $SBTi_6$ films. Each film shows a number of wedge shaped contrast parallel to the (001) plane of the substrate surface, which should be attributed to the large *c*-axis lattice constant, i.e., layered structure of each material is obtained.

Details of Figs. 8(a)–8(d) are shown in Figs. 9(a)–9(d), respectively. As can be seen in these figures, there are atomic shifts along [001] direction in all of the films. It should be noted that there are many such atomic shifts in the $SBTi_4$, $SBTi_5$, and $SBTi_6$ films while relatively few in the BTO films. Generally, such atomic shift and their different behavior in different films may be attributed to the following: First, different growth mode of BTO and $SBTi_m$ ($m=4$, 5, and 6) films results in the different density of atomic shift along [001] direction. Second, the step-like structure of the STO substrate surface and the local step-like defect of the films could also result in such an atomic shift.

As discussed above, at an early stage of film growth, each separated *c*-axis epitaxial $SBTi_m$ ($m=4$, 5, and 6) island grows independently, which means that the growth rate of each island is not necessary to be identical so with the film growing, when the neighboring islands become connected, the Bi_2O_2/perovskite/Bi_2O_2 sequence of each separated ep-

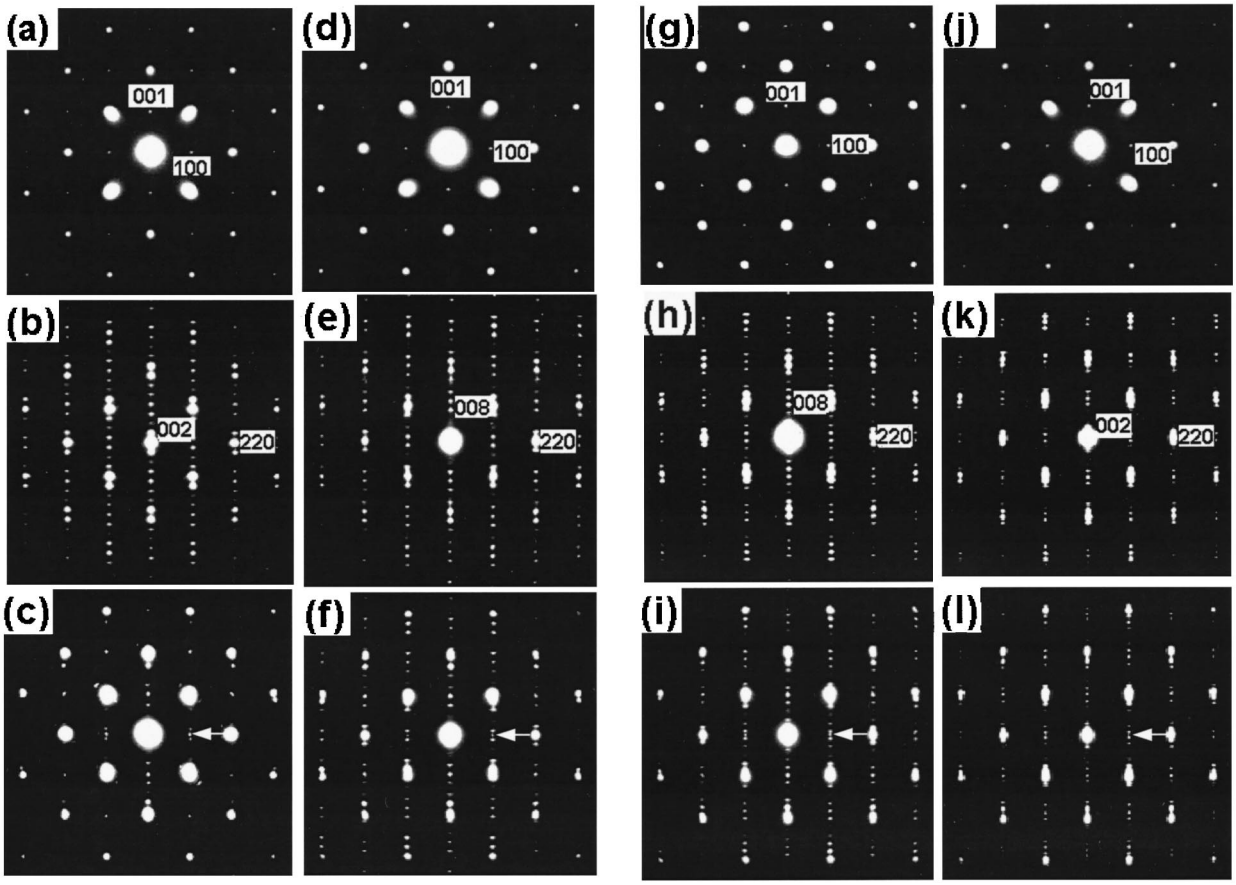

FIG. 7. Cross-sectional TEM overview of (a) BTO/STO, (b) $SBTi_4$/STO, (c) $SBTi_5$/STO, and (d) $SBTi_6$/STO heterostructures.

itaxial $SBTi_m$ ($m=4$, 5, and 6) island is different, resulting in the observed atomic shift along *c* axis as shown in Figs. 9(b)–9(d). This is consistent with the results observed in *c*-axis epitaxial $Ba_2Bi_4Ti_5O_{18}$ thin films.[16] In the case of 2D layer-by-layer grown BTO film, such an island connection will not occur. In this view, it seems that the BTO film should have no such atomic shift along [001] direction, however, as schematically shown in Fig. 10, the surface of (001) STO substrate can be considered to consist of a step, which will greatly affect the microstructure of 2D layer-by-layer grown BTO films if the height of the step is not the integer number of *c*-axis lattice constant, atomic displacement along the growth direction at the boundary of two neighboring steps. Therefore, the 2D layer-by-layer grown BTO films also have atomic shift along [001] direction. It should be noted that the step-like surface structure of (001) STO sub-

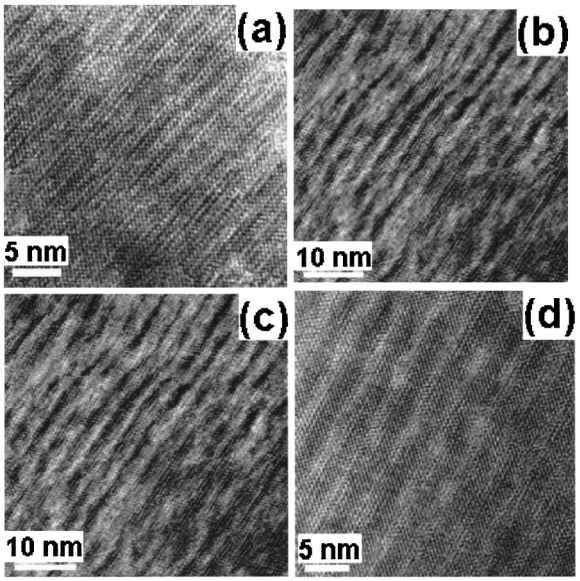

FIG. 8. HRTEM images of (a) BTO, (b) $SBTi_4$, (c) $SBTi_5$, and (d) $SBTi_6$ epitaxial films.

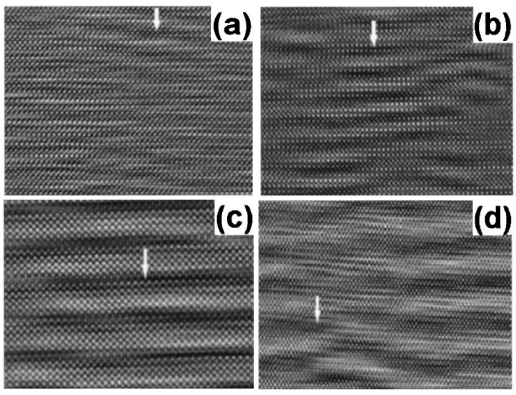

FIG. 9. Details of Fig. 7; (a) BTO, (b) $SBTi_4$, (c) $SBTi_5$, and (d) $SBTi_6$ epitaxial films.

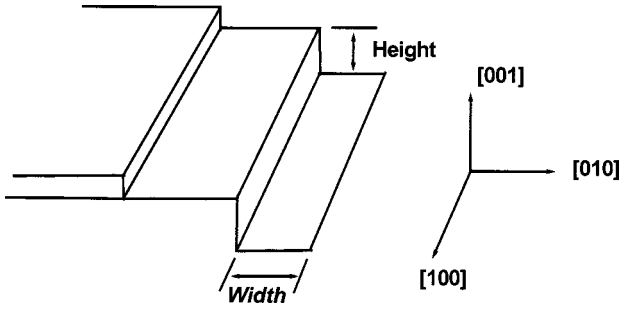

FIG. 10. Schematically surface structure of (001) STO single-crystal substrate.

strates could also affect the microstructure of $SBTi_m$ ($m=4$, 5, and 6) films. However, such influence may not be predominant compared with the influence resulted from the 3D island-like growth mode.

In these *c*-axis epitaxial films, a local distorted atomic line can be seen, as indicated by the white arrow in Fig. 9(a). It is reported that the TiO_6 octahedra of the Bi-layered oxide can tilt slightly along the four nominally equivalent *a* axis,[27,28] this tilting will lead to the atoms such as Ti bend upward, downward left, or right irrationally. The repeated small bent will form this type of distorted atomic line. In fact, it is believed that such tilting also exists in $SBTi_m$ ($m=4$, 5, and 6) films, as indicated by arrows but compared to the atomic shift along the [001] direction in these films, such tilting is not predominant.

The local cross-sectional HRTEM images of the *c*-axis epitaxial BTO, $SBTi_4$, $SBTi_5$, and $SBTi_6$ films are presented in Figs. 11(a)–11(d), respectively. The Sr and Ti columns have relatively low intensities, the Bi columns high intensities, while O columns are not seen. This is because of their different atomic number: $Z=38$, 22, 83, and 8 for Sr, Ti, Bi, and O, respectively. The Sr and Ti columns have little difference in intensity because of the close atomic numbers between them. For each material, the stacking blocks of the alternate Bi_2O_2 layers and TiO_6 octahedra can be identified. The Bi_2O_2 layers are indicated by *B* while the TiO_6 octahedra lie between two neighboring $(Bi_2O_2)^{2+}$ layers, which fit well with the corresponding schematic representation of the crystal structure shown in Figs. 1(a)–1(d), respectively. The equal spacing between the double Bi_2O_2 layers indicates a single-phase film. It should be noted that for each film, between double Bi_2O_2 layers, other Bi columns can be detected, which correspond to the Bi–Ti–O ferroelectric blocks. The measured *c*-axis lattice constants of $m=3-6$ films are 32.8, 40.4, 49.1, and 56.7 Å. No intergrowths are observed in the imaged area of $m=3$, 4, and 5 films. However, some intergrowth of the $m=6$ phase is observed in localized region.

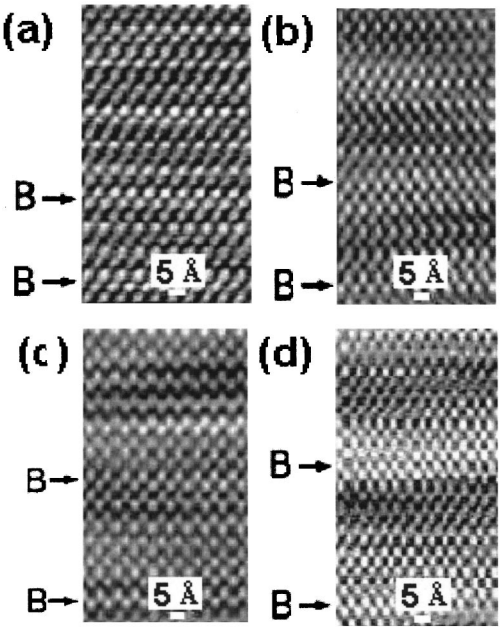

FIG. 11. HRTEM of a unit cell of the (a) BTO, (b) $SBTi_4$, (c) $SBTi_5$, and (d) $SBTi_6$.

IV. DIELECTRIC PROPERTIES

The growth of the *c*-axis epitaxial films allows the ε_{33} dielectric constants of these high anisotropic materials to be measured. Room temperature dielectric constants (ε_r) of these epitaxial films were measured with an evanescent microwave probe (EMP) to be 245 ± 23, 237 ± 13, 272 ± 19, and 221 ± 20. To confirm the results, the epitaxial films were grown directly on (001)-LAO single crystal substrates by PLD, respectively, because LAO has low dielectric constant (~24), which will not interfere with the dielectric measurement. The measured ε_r of the epitaxial films on LAO are 221 ± 13, 205 ± 15, 261 ± 29, and 249 ± 17 for $m=3$, 4, 5, and 6, respectively, which are comparable with the results measured on the films on STO substrates.

V. CONCLUSIONS

c-axis epitaxial thin films of homologous Bi-layered BTO, $SBTi_4$, $SBTi_5$, and $SBTi_6$ were fabricated on (001) STO single crystal substrates by PLD, respectively. Epitaxial relations were established to be

$$(001)Sr_{m-3}Bi_4Ti_mO_{3m+3}\|(001)SrTiO_3$$

and

$$[1\bar{1}0]Sr_{m-3}Bi_4Ti_mO_{3m+3}\|[010]SrTiO_3$$

($m=3$, 4, 5, and 6, respectively) by selected area diffraction (SAED) and x-ray ϕ scans. A special kind of atomic shift along [001] and a slight vibration of TiO_6 octahedra are revealed and discussed. The room-temperature dielectric constants of the epitaxial films measured by using an evanescent microwave probe were 245 ± 23, 237 ± 13, 272 ± 19, and 221 ± 20 for BTO, $SBTi_4$, $SBTi_5$, and $SBTi_6$ films, respectively.

ACKNOWLEDGMENTS

The authors would like to acknowledge discussion with and support from Dr. X.-D. Xiang and Dr. G. Wang in the EMP measurements. The work at Nanjing University was jointly supported by the National 863 High Technology Pro-

gram, the State Key Program for Basic Research of China and the National Nature Science Foundation of China (Contract No. 50225204). The work at the University of Michigan was supported by the National Science Foundation through Grant Nos. DMR 9875405 (CAREER, X.Q.P) and DMR/IMR 9704175.

[1] J. F. Scott and C. A. P. de Araujo, Science (Washington, DC, U.S.) **246**, 1400 (1989).
[2] K. Lijima, Y. Tomita, R. Takeyama, and I. Ueda, J. Appl. Phys. **60**, 361 (1990).
[3] M. H. Francombe and S. V. Krinnawamy, J. Vac. Sci. Technol. A **8**, 11382 (1990).
[4] C. A. Paz de Araujo, J. D. Cuchlaro, L. D. McMillan, M. C. Scott, and J. F. Scott, Nature (London) **374**, 627 (1995).
[5] B. H. Park, B. S. Kang, S. D. Bu, T. W. Noh, J. Lee, and W. Jo, Nature (London) **401**, 682 (1999).
[6] D. Wu, A. D. Li, T. Zhu, Z. F. Li, Z. G. Liu, and N. B. Ming, J. Mater. Res. **16**, 1325 (2001).
[7] S. T. Zhang, B. Yang, J. F. Webb, Y. F. Chen, Z. G. Liu, D. S. Wang, Y. Wang, and N. B. Ming, J. Appl. Phys. **92**, 4954 (2002).
[8] J. Lettieri, M. A. Zurbuchen, Y. Jia, D. G. Schlom, S. K. Streiffer, and M. E. Hawley, J. Appl. Phys. **76**, 2937 (2000).
[9] J. Withers, G. Thompson, and A. D. Rae, J. Solid State Chem. **94**, 404 (1991).
[10] Z. M. Satyalakshmi, M. Alexe, A. Pignolet, N. D. Zakharov, C. Harnagea, S. Senz, and D. Hesse, Appl. Phys. Lett. **74**, 603 (1999).
[11] Y. Yan, M. M. Al-Jassim, Z. Xu, X. Lu, D. Viehland, M. Payne, and S. J. Pennycook, Appl. Phys. Lett. **75**, 1961 (1999).
[12] U. Chon, H. M. Jang, M. G. Kim, and C. H. Chang, Phys. Rev. Lett. **89**, 087601 (2002).
[13] B. Aurivillius and P. H. Fang, Phys. Rev. **126**, 893 (1962).
[14] M. Tachiki, K. Yamamuro, and T. Kobayashi, Jpn. J. Appl. Phys., Part 2 **35**, L719 (1996).
[15] J. H. Haeni, C. D. Theis, D. G. Schlom, W. Tian, X. Q. Pan, H. Chang, I. Takeuchi, and X. D. Xiang, Appl. Phys. Lett. **78**, 3292 (2001).
[16] D. Hesse, N. D. Zakharov, A. Pignolet, A. R. James, and S. Senz, Cryst. Res. Technol. **35**, 641 (2000).
[17] C. Gao and X.-D. Xiang, Rev. Sci. Instrum. **69**, 3846 (1998).
[18] H. Chang, I. Takeuchi, and X.-D. Xiang, Appl. Phys. Lett. **74**, 1165 (1999).
[19] T. Suzuki, Y. Nishi, M. Fujimoto, K. Ishikawa, and H. Funakubo, Jpn. J. Appl. Phys., Part 2 **38**, L1262 (1999).
[20] Y. Ma, K. Watanabe, S. Awaji, and M. Motokawa, Phys. Rev. B **65**, 174528 (2002).
[21] C. Gerber, D. Anselmetti, J. G. Bednorz, J. Mannhart, and D. G. Schlom, Nature (London) **350**, 279 (1991).
[22] W. C. Goh, S. Y. Xu, S. J. Wang, and C. K. Ong, J. Appl. Phys. **89**, 4497 (2001).
[23] R. E. Cavicchi, S. Semancik, M. D. Antonik, and R. J. Lad, Appl. Phys. Lett. **61**, 1921 (1992).
[24] Y. F. Chen, L. Sun, T. Yu, J. X. Chen, N. B. Ming, D. S. Ding, and L. W. Wang, Appl. Phys. Lett. **67**, 3503 (1995).
[25] J. C. Jiang, Y. Lin, C. L. Chen, C. W. Chu, and E. I. Meletis, J. Appl. Phys. **91**, 3188 (2002).
[26] Y. Shimakawa, Y. Kubo, Y. Nakagawa, T. Kamiyama, H. Asano, and F. Izumi, Appl. Phys. Lett. **74**, 1904 (1999).
[27] D. J. Srolovitz and J. F. Scott, Phys. Rev. B **34**, 1815 (1986).
[28] J. F. Scott, *Ferroelectric Memories* (Springer, Berlin, 2000), p. 68.